Lattice dynamics of YVO_4 at high pressures

F. J. Manjón,[1,*] P. Rodríguez-Hernández,[2] A. Muñoz,[2] A. H. Romero,[3] D. Errandonea,[4] and K. Syassen[5]
[1]*Instituto de Diseño para la Fabricación y Producción Automatizada, MALTA Consolider Team, Universitat Politècnica de València, 46022 Valencia, Spain*
[2]*MALTA Consolider Team, Departamento de Física Fundamental II, Universidad de La Laguna, La Laguna, Tenerife, Spain*
[3]*CINVESTAV, Unidad Querétaro, Libramiento Norponiente 2000, 76230 Querétaro, Mexico*
[4]*MALTA Consolider Team, Fundación General de la Universitat de València, Edificio de Investigación, 46100 Burjassot, Valencia, Spain*
[5]*Max-Planck Institut für Festkörperforschung, Heisenbergstr. 1, 70569 Stuttgart, Germany*
(Received 6 October 2009; revised manuscript received 9 December 2009; published 3 February 2010)

We report an experimental and theoretical lattice-dynamics study of yttrium orthovanadate (YVO_4) up to 33 GPa together with a theoretical study of its structural stability under pressure. Raman-active modes of the zircon phase are observed up to 7.5 GPa, where the onset of an irreversible zircon-to-scheelite phase transition is detected, and Raman-active modes in the scheelite structure are observed up to 20 GPa, where a reversible second-order phase transition occurs. Our *ab initio* total-energy calculations support that the second-order phase transition in YVO_4 is from the scheelite to the monoclinic M-fergusonite structure. The M-fergusonite structure remains up to 33 GPa and on pressure release the sample reverts back to the metastable scheelite phase. Raman- and IR-mode symmetries, frequencies, and pressure coefficients in the zircon, scheelite, and M-fergusonite phases are discussed.

DOI: 10.1103/PhysRevB.81.075202 PACS number(s): 63.20.−e, 78.30.−j, 71.15.Mb

I. INTRODUCTION

Yttrium orthovanadate (YVO_4) is a well-known host for rare-earth ions and is used in solid-state lasers[1] and phosphors.[2] Rare-earth-doped YVO_4 has attracted much attention because of its application in highly efficient diode-pumped solid-state lasers; it exhibits a high absorption coefficient, large emission cross section, and long fluorescence lifetime.[3] Furthermore, highly efficient nanocrystalline phosphors based on YVO_4 doped with rare-earth ions have been recently synthesized and have paved the way for new applications to be developed.[4–6]

At room conditions YVO_4 bulk samples and nanocrystals with size down to 10 nm crystallize in the tetragonal zircon-type structure [space group (SG): D_{4h}^{19} or $I4_1/amd$, No. 141, $Z=2$].[4,7,8] In this structure, the V atoms are tetrahedrally coordinated by oxygen-forming VO_4 tetrahedra while Y atoms are eightfold coordinated by oxygen-forming YO_8 dodecahedra. Several Raman and infrared (IR) studies of the zircon phase at room pressure have been carried out[9–15] and the observed lattice modes have been analyzed using group theoretical models.[9,16,17]

Upon compression a transformation from the zircon to the scheelite structure (SG: C_{4h}^6 or $I4_1/a$, No. 88, $Z=4$) has been reported above 7.5 GPa (Refs. 18 and 19) and the pressure dependence of the Raman-active modes in both the zircon and the scheelite structures up to 14 GPa at room temperature (RT) is well documented.[18] However, this work did not report the observation of several Raman modes in the zircon and scheelite phases, neither it reported the phase transition from the scheelite to the M-fergusonite structure that has been recently found in high-pressure studies of zircon- and scheelite-type compounds.

In this work, we report RT Raman-scattering measurements in YVO_4 up to 33 GPa together with total-energy and lattice-dynamical *ab initio* calculations in the zircon, scheelite, and M-fergusonite (hereafter simply called fergusonite) phases. Our purposes are: (i) to assign the symmetry of the Raman modes of the zircon and scheelite phases; (ii) to clarify why several zone-center lattice modes have not been observed neither in the zircon nor in the scheelite-type structures; and (iii) to explore the stability region of the scheelite phase to check for a possible scheelite-to-fergusonite phase transition, as already predicted by crystal-chemical arguments[20,21] and recently found in several scheelites[22–25] and in several zircon-type orthovanadates such as $LuVO_4$, $YbVO_4$, and $EuVO_4$.[26–29]

II. EXPERIMENTAL DETAILS

We have used YVO_4 single crystals grown by the Czochralski method with 0.58% Nd concentration. These crystals were used in previous x-ray diffraction and luminescence measurements under pressure.[19,30] A sample (100 μm $\times$ 100 μm $\times$ 30 μm) was inserted in a diamond-anvil cell with a 4:1 methanol-ethanol mixture as pressure-transmitting medium, ensuring hydrostatic conditions up to 10 GPa and quasihydrostatic conditions between 10 and 33 GPa.[31,32] Pressure was determined by the ruby luminescence method.[33]

Two runs of unpolarized RT Raman-scattering experiments at high pressures in backscattering geometry were performed in different setups. In a first run, measurements up to 7 GPa were performed using an Ar^+-ion laser (5145 Å line) and a Jobin-Yvon T64000 triple spectrometer in combination with a multichannel charge-coupled device (CCD) detector with a spectral resolution around 1 cm^{-1} and measurements from 7 till 16 GPa were performed using a HeNe laser (6328 Å line) and a Dilor LabRam spectrometer in combination with a multichannel CCD detector with a spectral resolution around 3 cm^{-1}. In this run, pressure was released from 16 GPa and the Raman-active modes of the high-

TABLE I. Calculated (th.) and experimental (exp.) lattice parameters of the zircon and scheelite structures at ambient pressure and the calculated scheelite and fergusonite structures at 24.3 GPa. Bulk moduli for the zircon and scheelite structures of YVO_4 at ambient pressure calculated with a fourth-order Birch-Murnaghan equation of state are also reported for comparison with experimental values.

	a (Å)	b (Å)	c (Å)	β (deg)	B_0 (GPa)	B_0'	References
			Zircon (0 GPa)				
th.(LDA)	7.072		6.208		150.4	4.7	This work
th.(LDA)	7.051		6.203		142.8		Ref. 37
th.(GGA)	7.218		6.334		123.3	5.4	This work
th.(GGA)	7.179		6.313		122.0		Ref. 37
exp.	7.122		6.291		130	4.4	Ref. 19
			Scheelite (0 GPa)				
th.(LDA)	4.980		11.044		159.7	4.2	This work
th.(GGA)	5.080		11.348		144.4	3.8	This work
exp.	5.032		11.233		138	4.5	Ref. 19
			Scheelite (24.3 GPa)				
th.(LDA)	4.825		10.501				This work
			M-fergusonite (24.3 GPa)				
th.(LDA)	4.680	10.341	4.987	95.47			This work

pressure scheelite phase were measured down to ambient pressure where the scheelite phase is metastable. In a second run, measurements up to 33 GPa were performed using a Renishaw Invia spectrometer in combination with a TE-cooled multichannel CCD detector with a spectral resolution around 3 cm^{-1}. Since the sample orientation is not known in our measurements, the spectra should correspond to a mixture of the polarizations perpendicular and parallel to the c axis. Argon and helium plasma lines were used to calibrate the spectra in the different setups.

III. *AB INITIO* CALCULATIONS

In order to explore the relative stability of the zircon, scheelite, and fergusonite phases and their respective phase-transition pressures, we have performed *ab initio* total-energy calculations within the framework of the density-functional theory and the pseudopotential method using the Vienna *ab initio* simulation package (VASP) [see Ref. 34, and references therein]. The exchange-correlation energy was taken in both the local-density approximation (LDA) with the Ceperley-Alder prescription for the exchange energy and the generalized gradient approximation (GGA) with the PBE prescription.[35] The projector-augmented wave (PAW) scheme[36] was adopted and the semicore 4*s* and 4*p* electrons of Y and the semicore 3*s* and 3*p* electrons of V were dealt with explicitly in the calculations. The set of plane waves used extended up to a kinetic-energy cutoff of 1200 and 520 eV for LDA and GGA, respectively. These cutoffs were required to achieve highly converged results within the PAW scheme.[36] We use a dense Monkhorst-Pack grid for the Brillouin-zone (BZ) integrations to ensure highly converged results in the three phases (to about 1–2 meV/f.u.). We also use an accurate prescription during the calculations in order to obtain very well-converged forces during the calculation of the dynamical matrix. At each selected volume, the structures were fully relaxed to their equilibrium configuration through the calculation of the forces on atoms and the stress tensor.[24] In the relaxed equilibrium configuration, the forces on the atoms are less than 0.002 eV/Å and the deviation of the stress tensor from a diagonal hydrostatic form is less than 1 kbar (0.1 GPa). Table I shows the comparison between the experimental and calculated lattice parameters in the zircon and scheelite phases at room pressure. As usual, LDA calculations underestimate the experimental lattice parameters while GGA calculations overestimate them. GGA yields calculated bulk moduli for zircon-type YVO_4 in better agreement with experiment similarly to previous calculations.[37]

We have also performed lattice-dynamics calculations of the phonon modes in the zircon, scheelite, and fergusonite phases at the zone center (Γ point) of the BZ. Our theoretical results enable us to assign the Raman modes observed for the different phases of YVO_4. Further, the calculations provide information about the symmetry of the modes and polarization vectors which are not readily accessible in the present experiment. Highly converged results on forces are required for the calculation of the dynamical matrix. We use the direct force-constant approach (or supercell method).[38] The construction of the dynamical matrix at the Γ point of the BZ is particularly simple and involves separate calculations of the forces in which a fixed displacement from the equilibrium configuration of the atoms within the *primitive* unit cell is considered. Symmetry aids by reducing the number of such independent displacements, reducing the computational effort in the study of the analyzed structures considered in this work. Diagonalization of the dynamical matrix provides both the frequencies of the normal modes and their polarization vectors. It allows us to identify the irreducible representation and the character of the phonons modes at the Γ point. In the

following, we will refer to Raman-active modes only. The calculated frequencies and pressure coefficients of the infrared-active modes for the three phases of YVO_4 are given as supplementary material of this paper.[39]

IV. RESULTS AND DISCUSSION

A. Zircon-type YVO_4

The zircon structure of YVO_4 has two formula units per primitive cell, thus supporting 36 zone-center modes which decompose in the irreducible representations of D_{4h} symmetry as follows:[9]

$$\Gamma_{36} = (2A_{1g} + 2B_{1u}) + (4B_{1g} + 4A_{1u}) + (A_{2g} + B_{2u}) + (B_{2g} + A_{2u}) + (5E_g + 5E_u). \quad (1)$$

The pairs of species enclosed in parenthesis derive from the same motion of the YVO_4 molecule. The two acoustic branches come from A_{2u} and E_u modes while the rest correspond to optic modes. The first mode of the pairs is even and the second odd with respect to inversion so the first member of the pairs is Raman active and the second is IR active. Since the A_{2g} mode is a silent mode, we expect only 12 zone-center Raman-active modes.

The vibrational modes of the ABO_4 compounds can be classified either as internal or external modes of the BO_4 unit. The external modes either correspond to a pure translation (T) or to a pure rotation (R) of the BO_4 molecule while the internal modes can be decomposed into four types of motion (ν_1, ν_2, ν_3, and ν_4) on the light of the T_d symmetry of the BO_4 molecule.[40] The reduction in the representation of T_d symmetry under the D_{2d} symmetry of the VO_4 site in the zircon lattice of YVO_4 and the transformation of the D_{2d} representation to the D_{4h} representation yields the following 12 zone-center Raman-active modes:

$$\Gamma = \nu_1(A_g) + \nu_2(A_g) + \nu_2(B_{2g}) + \nu_3(B_g) + \nu_3(E_g) + \nu_4(B_g) + \nu_4(E_g) + R(E_g) + 2T(B_g) + 2T(E_g). \quad (2)$$

The external translational and rotational modes are the lowest in frequency whereas the internal modes are the highest in frequency. Several works reported 10 out of the 12 Raman-active modes in YVO_4; being nonobserved two E_g modes.[9–12] This is in good agreement with the most recent measurements already reported.[13] However, Jayaraman *et al.* reported and followed under pressure the evolution of only 9 out of the 12 Raman-active modes of the zircon-type phase of YVO_4,[18] and they considered that the unobserved Raman modes were one translational mode $T(B_g)$, the rotational mode $R(E_g)$, and the internal mode $\nu_4(E_g)$.

Figure 1(a) shows the experimental Raman spectra of zircon-type YVO_4 at different pressures up to 6 GPa, which is below the upstroke zircon-scheelite phase transition at 7.5 GPa. We have observed and followed under pressure nine Raman modes similarly to Jayaraman *et al.*[18] The first-order Raman modes of the zircon phase show a phonon gap between 500 and 800 cm^{-1}, with modes between these wave numbers and above 950 cm^{-1} being likely second-order modes. Similar Raman spectra have been found in $DyVO_4$ and $TbVO_4$.[41] Figure 1(b) shows the experimental pressure dependence of the frequencies of the nine first-order Raman modes plus three Raman modes (a,b,c) that likely correspond to second-order modes in zircon-type YVO_4. We have

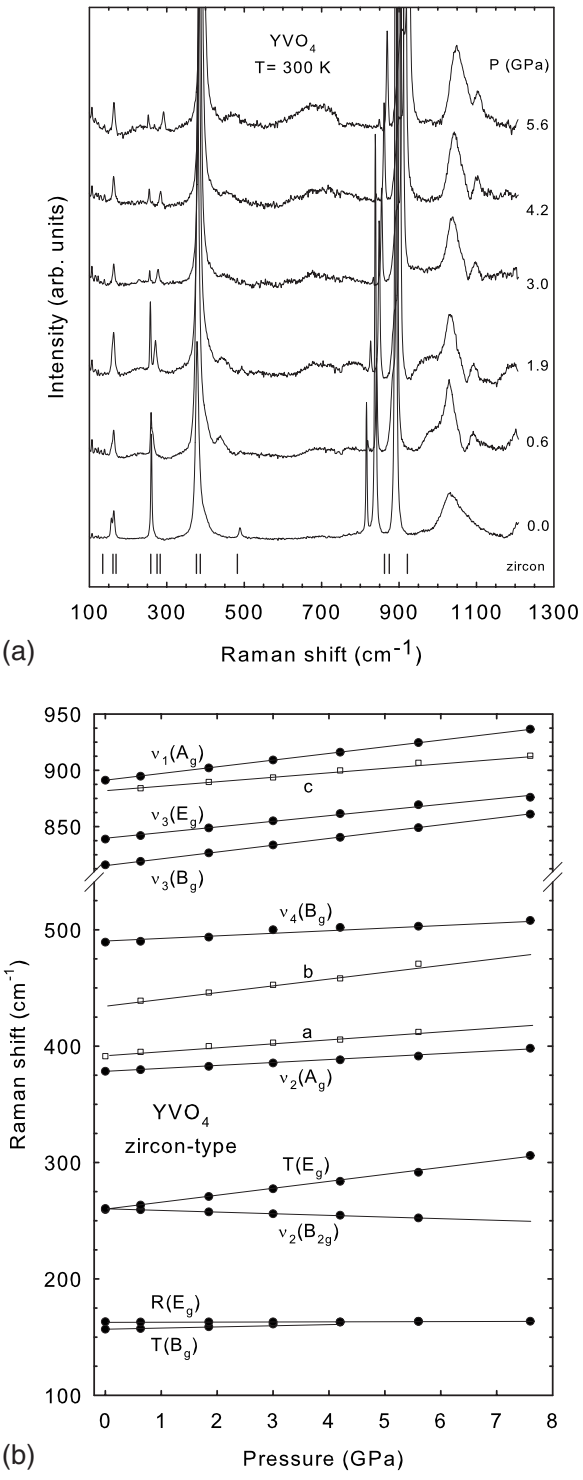

FIG. 1. (a) Experimental Raman spectra in zircon-type YVO_4 at pressures between 1 atm and 6 GPa. Bottom marks indicate the LDA-calculated frequencies of the Raman-active modes in the zircon phase at 1 atm. (b) Experimental pressure dependence of the Raman-mode frequencies in zircon-type YVO_4. Empty squares are likely second-order modes.

TABLE II. Experimental Raman-mode frequencies and pressure coefficients observed in zircon-type YVO_4 at room temperature as obtained from fits to the data using $E(P)=E(0)+a_1P$. Theoretical (th.) values calculated both in the LDA and GGA are also shown for comparison.

Mode	ω_0 (cm^{-1})	a_1 (cm^{-1}/GPa)	ω_0 (th.)[a] (cm^{-1})	a_1 (th.)[a] (cm^{-1}/GPa)	ω_0 (th.)[b] (cm^{-1})	a_1 (th.)[b] (cm^{-1}/GPa)
$T(E_g)$			134	−0.30	131	0.38
$R(A_{2g})$	Silent		163	−2.47	172	−2.36
$T(B_g)$	156.8	1.33	163	0.57	150	1.50
$R(E_g)$	163.2	0.05	168	0.31	157	−0.81
$\nu_2(B_{2g})$	259.6	−1.30	256	−1.53	255	−1.54
$T(B_g)$			274	3.25	252	3.11
$T(E_g)$	260.5	5.62	276	5.01	238	6.62
$\nu_4(E_g)$			376	0.82	371	0.68
$\nu_2(A_g)$	378.4	2.34	380	3.33	360	1.94
$\nu_4(B_g)$	489.3	2.77	480	2.90	461	2.79
$\nu_3(B_g)$	816.0	5.93	862	6.03	811	6.11
$\nu_3(E_g)$	838.8	5.46	874	4.91	825	5.68
$\nu_1(A_g)$	891.1	5.99	924	3.45	875	6.31

[a]LDA.
[b]GGA.

identified one Raman mode with negative pressure coefficient while our calculations yield mainly negative pressure coefficients for two zircon-type Raman-active modes in YVO_4: a $T(E_g)$ mode and the $\nu_2(B_g)$ mode. The presence of two modes with negative pressure coefficient was also observed in zircon-type $YbVO_4$ (Ref. 29) and in zircon-type $DyVO_4$ and $TbVO_4$.[41] Note that in Ref. 41, the $\nu_2(B_g)$ mode was incorrectly assigned to a $T(E_g)$ mode and vice versa.

Table II summarizes the experimental and theoretical first-order Raman-mode frequencies and pressure coefficients at room pressure in the zircon phase. Our Raman frequencies at room pressure agree with those of previous works[9–13,18] and our pressure coefficients agree with those of previous high-pressure measurements.[18] Also a good agreement between experimental and theoretical calculations is found. Furthermore, our *ab initio* calculations have allowed us to assign the symmetries of the observed modes in the zircon phase. As already commented, previous authors did not observe two E_g modes in YVO_4.[9–13] However, Jayaraman noted the lack of an additional $T(B_g)$ mode.[18] Our calculations indicate that the nonobserved modes are the highest-frequency $T(B_g)$ mode, whose frequency is very close to either the high-frequency $T(E_g)$ or to the $\nu_2(B_{2g})$ mode and the $\nu_4(E_g)$ mode, whose frequency is very close to that of the $\nu_2(A_g)$ mode. This means that the nonobserved modes could be easily masked by the high Raman intensity of the neighboring modes. On the other hand, our calculations indicate that the third nonobserved mode in the zircon phase could be the $T(E_g)$ mode of lower frequency, whose calculated frequency at ambient pressure is around 130 cm^{-1} and which should exhibit a negligible pressure coefficient. The lack of observation of this last mode agrees with Refs. 9–13, and it is in disagreement with Jayaraman *et al.* who assumed that the nonobserved mode was the $R(E_g)$ mode that we have assigned to the Raman band near 163 cm^{-1} in good agreement with Refs. 9–13.

B. Scheelite-type YVO_4

YVO_4 undergoes a zircon-to-scheelite phase transition near 7.5 GPa.[18,19] The scheelite structure of YVO_4 has four formula units per body-centered unit cell where Y and V atoms occupy S_4 sites and the 16 O atoms are on C_1 sites. Group theoretical considerations predict the following representation:[17]

$$\Gamma_{24} = (3A_g + 3B_u) + (5B_g + 5A_u) + (5E_g + 5E_u). \quad (3)$$

Consequently, we expect 13 zone-center Raman-active modes that can also be classified as internal or external modes of the BO_4 molecule and that can be expressed as

$$\Gamma = \nu_1(A_g) + \nu_2(A_g) + \nu_2(B_g) + \nu_3(B_g) + \nu_3(E_g) + \nu_4(B_g) + \nu_4(E_g) + R(A_g) + R(E_g) + 2T(B_g) + 2T(E_g). \quad (4)$$

Figure 2(a) shows the experimental Raman spectra of scheelite-type YVO_4 at different pressures from ambient pressure up to 16 GPa. The spectra of the scheelite phase below 7.5 GPa have been measured on pressure release from 16 GPa since the scheelite phase is metastable at ambient conditions and does not return to the zircon phase on decreasing pressure. Similar to the zircon phase, the Raman modes of the scheelite phase exhibit a phonon gap between 500 and 700 cm^{-1}, as already observed and discussed in scheelite-type tungstates.[24,25] On this basis, we assign the Raman modes between 500 and 700 cm^{-1} and above 850 cm^{-1} to second-order modes. Figure 2(b) shows the experimental pressure dependence of the frequencies of the 13 Raman-active modes in scheelite-type YVO_4.

Table III summarizes the experimental and theoretical first-order Raman-mode frequencies and pressure coefficients at room pressure in the scheelite phase of YVO_4. Our experimental data agree with those of Ref. 18 and a good overall agreement between experimental and calculated val-

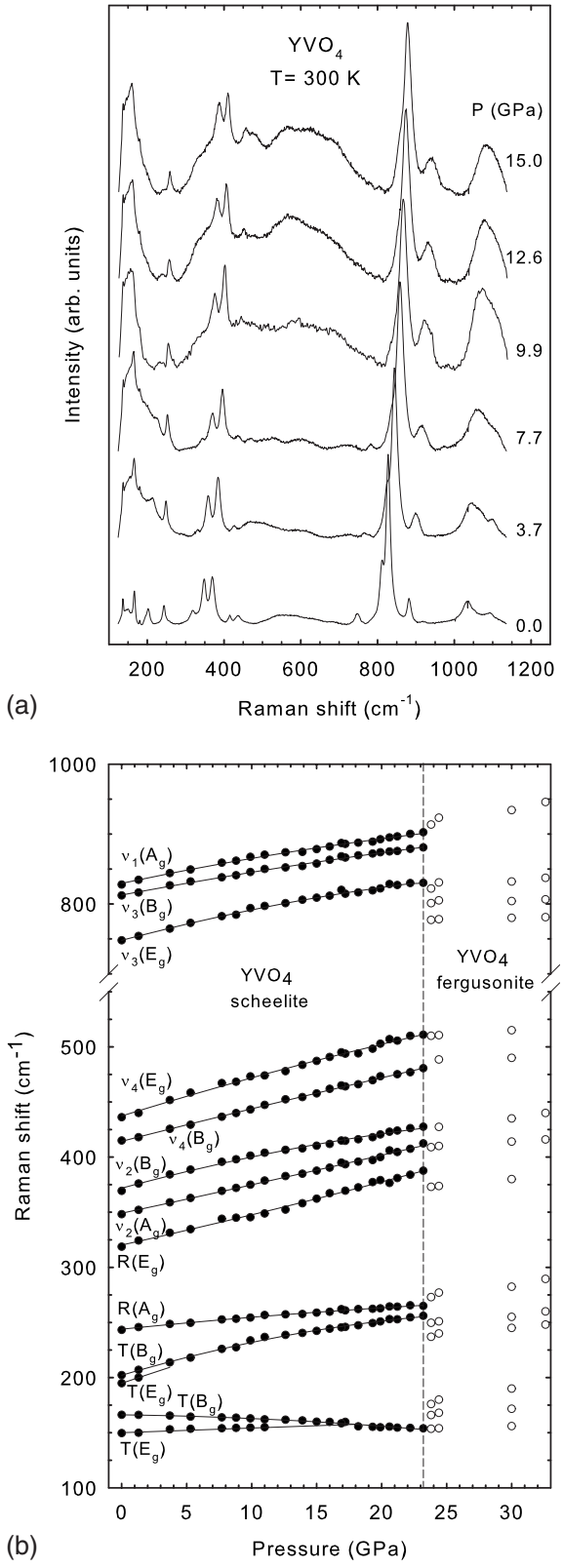

FIG. 2. (a) Experimental Raman spectra of the high-pressure phases of YVO_4 at pressures between 1 atm and 15 GPa. (b) Experimental pressure dependence of the Raman-mode frequencies in scheelite-type YVO_4 (filled circles) and M-fergusonite YVO_4 (empty circles). The vertical dashed line indicates the experimentally measured phase-transition pressure from the scheelite to the M-fergusonite phase.

ues is found. Only the lowest-frequency $T(B_g)$ mode exhibits a negative pressure coefficient in very good agreement with our theoretical calculations. Possible implications of the negative shift of this mode are addressed in the next section in relation to the Landau theory of phase transitions.

Previous measurements reported only 12 out of the 13 Raman-active modes of the scheelite-type phase of YVO_4.[18] It was assumed that one translational $T(B_g)$ mode was the only not-observed mode. Lattice-dynamics calculations support the symmetry assignment of the Raman-active modes in the scheelite phase already done by Jayaraman *et al.* with the only exception of the highest-frequency $T(B_g)$ and $T(E_g)$ modes. Our calculations differ in the ordering of these two modes with similar frequencies and pressure coefficients. It is one of these two modes the only one that was not observed by Jayaraman *et al.*[18] In fact, a close inspection of the spectra near ambient pressure allows to see that the mode near 202 cm^{-1} is indeed a double mode with a shoulder near 195 cm^1 [see inset of Fig. 3(a)]. We have tentatively attributed the two modes at 195 and 202 cm^{-1} to the previously nonobserved $T(B_g)$ mode and the $T(E_g)$ mode, respectively. Unfortunately, the weak intensity of the first mode and the appearance of a broad band in the Raman spectra above 3 GPa have prevented us from measuring its whole pressure dependence.

Our total-energy calculations predict a zircon-to-scheelite phase transition occurring at a pressure of 0.9 GPa (LDA) or 5.0 GPa (GGA) in contrast to the 7.5 GPa observed experimentally. The LDA value agrees with previous estimations of the thermodynamic equilibrium pressure (1–2 GPa) for the zircon-to-scheelite transition in several compounds[18,42] while the GGA value agrees better with the experimental phase-transition pressure. Recently, a general formula relating phase-transition pressure with the R_{BO_4}/R_A ionic radii ratio for ABO_4 compounds has been proposed.[43] The formula accounts well for the phase-transition pressure in scheelite-type compounds but it has been found not usable for zircon-type structures.[28] Indeed, a pressure between 7 and 9 GPa is necessary for the zircon-to-scheelite transition to take place in most zircon-type ABO_4 compounds irrespective of the A ion. This overpressure is likely the energy barrier that has to be overcome in the reconstructive transition proposed by Kusaba *et al.*[44] and recently confirmed by Marqués *et al.*[45,46] Finally, we want to comment that many facts suggest that zircon-type compounds at room conditions could be high-temperature phases quenched during crystal growth. This is suggested by (i) many scheelite-type compounds transform to the zircon structure on increasing temperature and (ii) all zircon-type compounds undergoing a pressure-induced phase transition toward the scheelite phase are observed to remain in the scheelite phase on decreasing pressure at room conditions. Therefore, the question of whether zircon or scheelite is the thermodynamically stable structure at room conditions in many ABO_4 compounds is not clearly resolved yet.

C. Fergusonite-type YVO_4

The pressure-induced scheelite-to-fergusonite phase transition is in good agreement with crystal-chemical

TABLE III. Experimental Raman-mode frequencies and pressure coefficients observed in scheelite-type YVO_4 at room temperature as obtained from fits up to 20 GPa using $E(P)=E(0)+a_1P+a_2P^2$. Theoretical (th.) *ab initio* values for the frequencies and zero-pressure coefficients calculated with LDA and GGA are also shown for comparison.

Mode	ω_0 (cm^{-1})	a_1 (cm^{-1}/GPa)	a_2 (cm^{-1}/GPa^2)	ω_0 (th.)[a] (cm^{-1})	a_1 (th.)[a] (cm^{-1}/GPa)	ω_0 (th.)[b] (cm^{-1})	a_1 (th.)[b] (cm^{-1}/GPa)
$T(E_g)$	148.9	1.00	−0.05	152	0.27	143	1.37
$T(B_g)$	166.2	−0.16	−0.02	157	−1.51	162	−0.33
$T(B_g)$	194.9	3.90		220	3.50	189	4.26
$T(E_g)$	202.2	3.49	−0.05	209	2.94	190	3.67
$R(A_g)$	243.9	1.19	−0.01	244	−1.62	232	1.22
$R(E_g)$	320.2	2.62	0.01	324	2.86	300	3.84
$\nu_2(A_g)$	349.1	2.53	0.005	348	3.24	327	3.07
$\nu_2(B_g)$	371.8	3.20	−0.04	374	3.05	349	3.59
$\nu_4(B_g)$	414.3	3.02	−0.07	411	1.94	397	3.24
$\nu_4(E_g)$	437.3	3.67	−0.02	435	3.25	413	3.01
$\nu_3(E_g)$	747.8	4.94	−0.06	784	4.34	741	4.75
$\nu_3(B_g)$	812.7	3.49	−0.02	833	4.06	794	6.48
$\nu_1(A_g)$	829.4	3.94	−0.04	845	7.60	814	3.11

[a]LDA.
[b]GGA.

considerations[20,21] and is common in many tungstates and halides.[24,25,47,48] Recently, the second-order character of this transition has been proved using Landau's theory of phase transitions in several scheelite-type tungstates and molybdates.[49,50] Concerning vanadates, recent experimental and theoretical works have found a scheelite-to-fergusonite phase transition in zircon-type $LuVO_4$ occurring above 16 GPa after the zircon-to-scheelite phase transition occurring above 8 GPa.[26,27] This phase transition has also been recently observed in $EuVO_4$ and in $YbVO_4$.[28,29]

The monoclinic M-fergusonite structure is centrosymmetric and has space group $I2/a$ (C_{2h}^6) with four formula units per conventional unit cell (i.e., two formula units per primitive unit cell). Group theoretical considerations indicate that fergusonite-type YVO_4 should have 36 vibrational modes at the zone center of the BZ with the following representation:

$$\Gamma_{36} = (8A_g + 8A_u) + (10B_g + 10B_u). \quad (5)$$

The 18 gerade (g) modes are Raman active and the 18 ungerade (u) modes are IR active. The 18 Raman-active modes derive from the reduction in the tetragonal C_{4h} symmetry of the scheelite structure to the monoclinic C_{2h} symmetry of the fergusonite structure. In particular, every A_g and every B_g scheelite mode transforms into an A_g mode of the monoclinic symmetry while every doubly degenerate E_g scheelite mode transforms into two B_g modes. Therefore, there is a close relationship between the modes of the scheelite and the fergusonite phases.

Figure 4 shows experimental Raman spectra of YVO_4 from 16 to 33 GPa. A sudden change in the Raman spectrum is already noted at 20.6 GPa where a new high-frequency peak appears at 878 cm^{-1}. Further changes follow in the spectra at 23.8 GPa with the disappearance of several scheelite-type Raman modes [the two ν_2 modes between 400 and 430 cm^{-1} and the $\nu_3(E_g)$ mode at 828 cm^{-1} at 20.6 GPa]. Simultaneously, a broad band centered around 820 cm^{-1} appears at 23.8 GPa and it extends asymmetrically to lower frequencies. In order to check whether the changes in the Raman spectra occurring above 20 GPa are consistent with the onset of the fergusonite phase, we plot in Fig. 3(b) the experimental Raman spectrum at 23.8 GPa and compare it with the LDA calculated frequencies at 25 GPa for the scheelite and fergusonite phases. It can be observed that the experimental spectrum seems to be more compatible with the calculated frequencies for the fergusonite phase than with those of the scheelite phase. A strong evidence of the presence of the fergusonite structure is the change in the high-frequency modes with the appearance of Raman modes at smaller frequencies than that of the $\nu_3(E_g)$ mode of the scheelite phase. Therefore, the changes in the Raman spectra above 20 GPa are consistent with the splitting of the E_g modes expected for the scheelite-to-fergusonite transition. This splitting has been also observed in the pressure-induced transitions of scheelite tungstates $CaWO_4$, $SrWO_4$, $PbWO_4$, and $BaWO_4$.[24,25] Figure 2(b) shows the pressure dependence of the Raman modes of the fergusonite phase between 23.8 and 33 GPa. Table IV summarizes the experimental and theoretical Raman-mode frequencies and pressure coefficients in fergusonite YVO_4 at 25 GPa. Experimental and calculated frequencies and pressure coefficients for the fergusonite phase agree reasonably well.

Recent high-pressure Raman measurements in $BaWO_4$ and $PbWO_4$ evidenced the different coordination of W in the fergusonite phase.[24,25] In order to know the coordination of V in the fergusonite phase of YVO_4 we can use the diatomic approximation used by Hardcastle and Wachs. According to these authors, the internal stretching modes of the VO_4 tet-

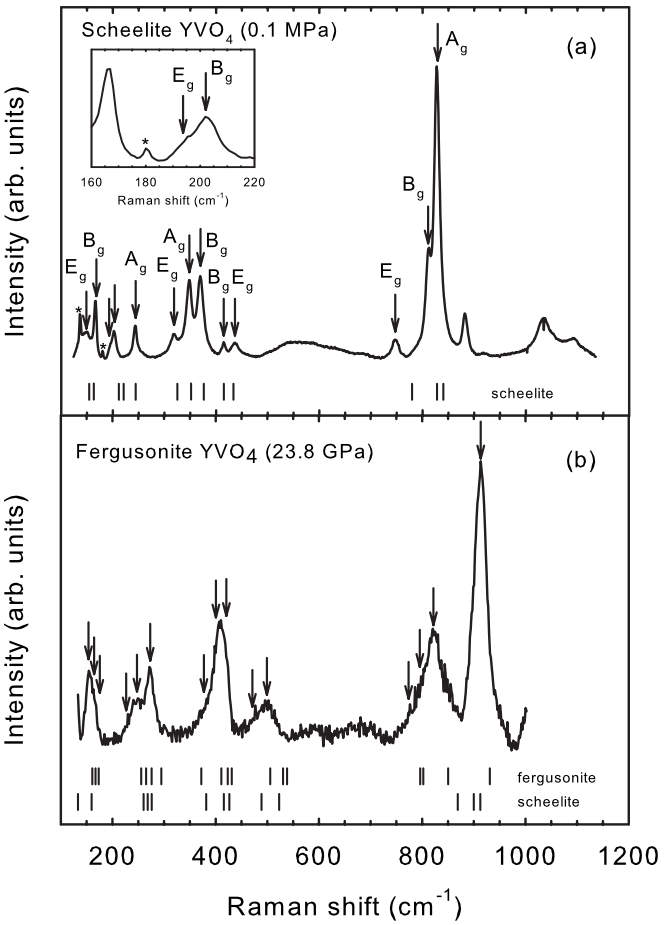

FIG. 3. (a) Experimental Raman spectrum of scheelite-type YVO_4 at 1 atm, where arrows indicate the first-order phonons and asterisks indicate the He plasma lines. Bottom marks indicate the LDA-calculated frequencies of the Raman-active modes in the scheelite phase at 1 atm. The inset shows the double-peak nature of the Raman feature near 200 cm^{-1}. (b) Experimental Raman spectrum of YVO_4 at 23.8 GPa. Arrows indicate new modes of the fergusonite phase while asterisks indicate modes left over from the scheelite phase. Bottom marks indicate the LDA-calculated frequencies at 25 GPa for the scheelite and fergusonite phases. A better agreement with the fergusonite phase can be observed specially at high frequencies.

rahedra in the zircon and scheelite phases are directly related to the bonding force and distance of the V-O bonds and they should reflect the fourfold coordination in agreement with the valence of the V cation.[51] Following Brown and Wu, who established a relationship between the bond distance R (in Å) and the Pauling's bond strengths,[52] it is possible to obtain an empirical relationship between the Raman stretching-mode frequencies and the Pauling's V-O bond strengths

$$s_{\text{V-O}} = [0.2912 \ln(21349/\omega)]^{-5.1}. \quad (6)$$

In this way, following Hardcastle and Wachs, it is possible to estimate the coordination of the V ion in a vanadium-oxide material if one knows all the stretching frequencies of the material, that usually fall in the high-frequency region above 400 cm^{-1}, and one sums the corresponding bond strengths

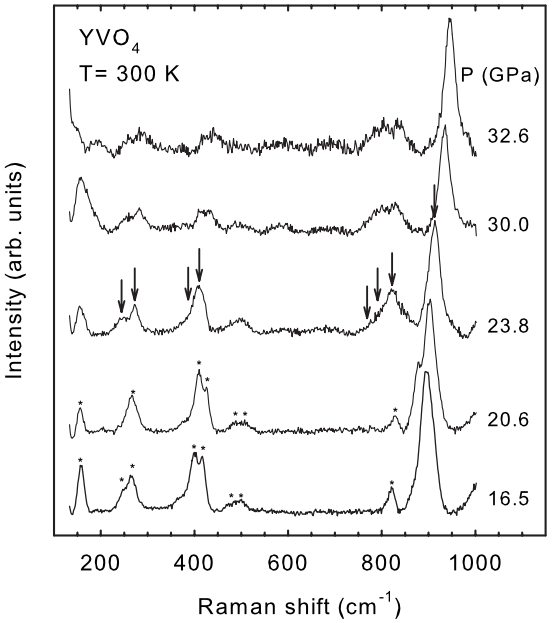

FIG. 4. Experimental Raman spectra of the high-pressure phases of YVO_4 at pressures between 16 and 33 GPa. Arrows indicate new modes of the fergusonite phase while asterisks indicate still modes of the scheelite phase.

for each stretching mode.[51] At room pressure, the three stretching modes are at 816, 838, and 891 cm^{-1} in the zircon phase of YVO_4 and Eq. (6) yields 5.6 v.u. (when the last mode is counted twice) that clearly deviates from the 5 valence of V despite we know about the fourfold coordination of V in the zircon phase. Similarly, the three stretching modes in the scheelite phase of YVO_4 are at 747, 813, and 829 cm^{-1} at room pressure and Eq. (6) yields 5.1 v.u. (when the last mode is counted twice) that match perfectly with the fourfold coordination of V in the scheelite phase. Jayaraman *et al.* already noted the strong decrease in frequency of the high-frequency stretching modes of the zircon phase in YVO_4 after the zircon-to-scheelite transition.[18] This strong decrease can be interpreted in terms of an increase in the V-O bond length in the scheelite phase compared to zircon, in good agreement with already reported diffraction measurements.[19] The normal value of 5.1 v.u. for scheelite YVO_4 and the anomalously high value of 5.6 v.u. for zircon YVO_4 also rises the doubt about the metastability of the zircon phase at room conditions as already commented in the previous section. Finally, as regards the coordination of the V ion in the fergusonite phase, our calculated frequencies for the fergusonite phase [see Table IV and Fig. 3(b)] support the assignment of the four stretching modes located at 780, 790, 830, and 910 cm^{-1} at 25 GPa. With these four modes and Eq. (6) one gets 5.3 v.u., which are consistent with a fourfold coordination of V at this pressure in fergusonite YVO_4.

Figure 5 shows the GGA calculations for the enthalpy vs volume in the zircon, scheelite, and fergusonite phases of YVO_4. Our total-energy calculations (for both LDA and GGA) predict the onset of the scheelite-to-fergusonite phase transition at 19 GPa in good agreement with the 20.6 GPa derived from our Raman measurements. Figure 6(a) shows the calculated deviation of the monoclinic beta angle of the

TABLE IV. Experimental Raman-mode frequencies and pressure coefficients observed in M-fergusonite-type YVO_4 at 25 GPa as obtained from fits using $E(P)=E(25\ \text{GPa})+a_1P$. Theoretical (th.) *ab initio* values calculated with LDA and GGA at 25 GPa are also shown for comparison.

Feature	ω_0 (cm^{-1})	a_1 (cm^{-1}/GPa)	ω_0 (th.)[a] (cm^{-1})	a_1 (th.)[a] (cm^{-1}/GPa)	ω_0 (th.)[b] (cm^{-1})	a_1 (th.)[b] (cm^{-1}/GPa)
F1(B_g)	154	0.38	162	1.19	155	−0.22
F2(A_g)	169	0.81	170	3.98	151	0.31
F3(B_g)	180	2.07	175	2.75	157	0.44
F4(A_g)	241	1.44	258	1.73	255	0.76
F5(B_g)	251	1.65	267	2.70	252	1.87
F6(A_g)			277	−0.03	260	1.80
F7(B_g)	278	1.53	296	2.73	254	2.30
F8(B_g)	374	1.12	374	0.78	360	1.74
F9(A_g)	411	1.07	412	1.13	390	2.13
F10(A_g)	427	1.92	429	1.87	409	1.87
F11(B_g)			432	3.48	363	2.09
F12(B_g)	489	0.27	509	1.05	491	3.19
F13(B_g)	511	0.84	537	2.00	493	4.47
F14(A_g)			546	5.57	464	3.02
F15(B_g)	778	0.45	796	−2.53	830	2.82
F16(A_g)	804	0.23	796	−0.21	869	2.30
F17(B_g)	831	1.24	852	0.98	834	3.02
F18(A_g)	924	3.14	940	2.83	889	2.39

[a]LDA.
[b]GGA.

fergusonite phase from 90° in the scheelite phase. The beta angle increases rapidly from 90° to 95° in the 19–24 GPa range for the LDA calculations while it increases slowly in the same pressure range for the GGA ones. These results indicate that the stable fergusonite phase is not reached up to 24 GPa at least in the LDA calculations and this allows to explain appearance of the strange Raman mode observed at 870 cm^{-1} at 20.6 GPa as coming from the restructuration of the beta angle between the scheelite and fergusonite phases. Figure 6(b) shows the LDA-calculated pressure dependence of the lattice parameters in the scheelite and fergusonite phases in YVO_4 between 10 and 35 GPa. The experimental pressure dependence of the lattice parameters in the scheelite phase after Ref. 19 is also shown for comparison. As observed in Fig. 6(b) and in Table I, LDA values usually underestimate the experimental lattice parameters while GGA values overestimate them; however, both calculations exhibit similar pressure dependence of the lattice parameters so GGA calculations are not shown in Fig. 6(b) for the sake of clarity. It can be observed that the a,b,c lattice parameters of the scheelite phase transform into the a,c,b lattice parameters of the fergusonite phase in good agreement with the transition sequence already reported for other scheelites undergoing the pressure-induced scheelite-to-fergusonite transition.

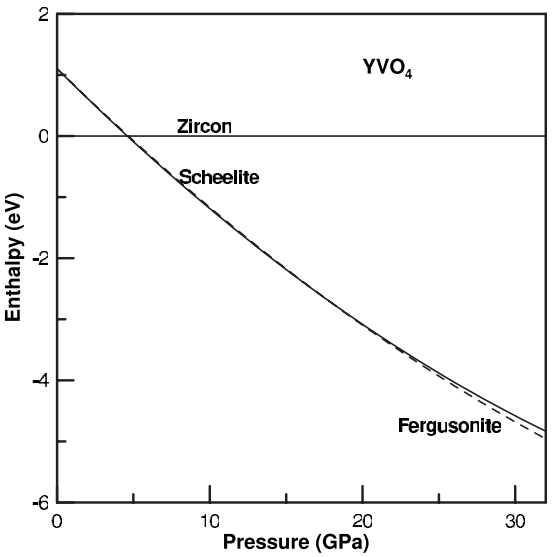

FIG. 5. Theoretical GGA calculation of enthalpy vs pressure for the zircon, scheelite, and M-fergusonite phases in YVO_4. The zircon-to-scheelite and scheelite-to-fergusonite phase transitions are predicted around 5 and 19 GPa, respectively, in contrast to LDA calculations that predict them around 1 and 19 GPa, respectively.

In order to shed light onto the nature of the scheelite-to-fergusonite phase transition, we have analyzed the spontaneous strain induced by pressure in the fergusonite structure applying Landau theory of phase transitions. Recently, this analysis has allowed to conclude that the scheelite-to-fergusonite transition in tungstates and molybdates is a second-order ferroelastic phase transition.[51–53] Support for the occurrence of the second-order scheelite-to-fergusonite

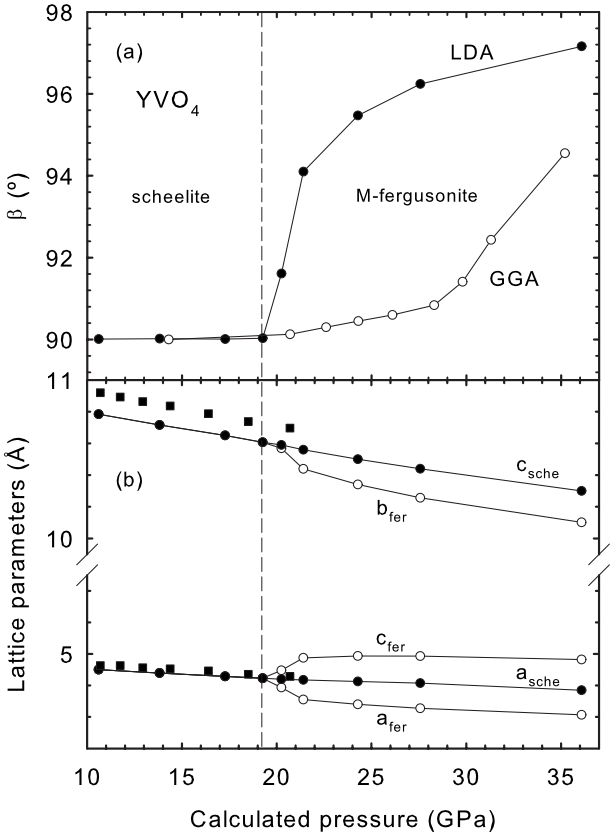

FIG. 6. (a) LDA- and GGA-calculated pressure dependence of the monoclinic β angle in the M-fergusonite phase of YVO_4 between 10 and 35 GPa. At pressures below 19 GPa the angle is 90° corresponding to the scheelite phase. (b) LDA-calculated pressure dependence of the lattice parameters of the scheelite (filled circles) and M-fergusonite (empty circles) phases between 10 and 35 GPa. Experimental data from Ref. 19 for the scheelite phase (full squares) is given for comparison. The vertical dashed line indicates the phase-transition pressure from the scheelite to the M-fergusonite phase. GGA values are not included in the figure for the sake of clarity.

phase transition in YVO_4 comes from the following observations: (i) there is no abrupt shift in Raman frequencies at the phase transition; (ii) there is no abrupt shift in volume;[26,27] (iii) there is a complete reversibility of the phase transition observed at 20 GPa, as observed from the recovery of the Raman modes of the scheelite phase below this pressure; and (iv) there is a scheelite-type $T(B_g)$ mode with negative pressure coefficient, as already observed in scheelite tungstates and molybdates in good agreement with Landau's theory of phase transitions.

According to Landau theory of phase transitions, second-order ferroelastic phase transitions should exhibit a soft mode, ω_P, in the paraelastic phase (scheelite phase in YVO_4) and a corresponding mode, ω_F, in the ferroelastic phase (fergusonite phase in YVO_4) with the following pressure dependences:[54]

$$\omega_P^2 = \kappa_P|P - P_P| \quad \omega_F^2 = \kappa_F|P - P_F|, \tag{7}$$

where κ_P and κ_F are constants, and P_P and P_F are the pressures at which the modes of each phase become unstable.

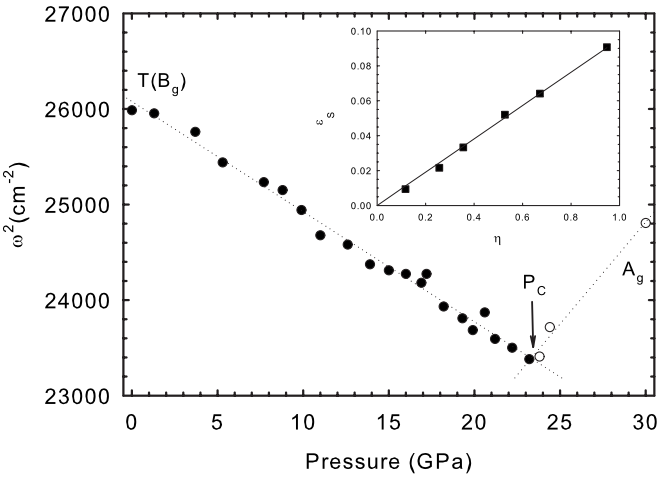

FIG. 7. Pressure dependence of the squared frequency of the $T(B_g)$ soft mode in the scheelite phase and the corresponding A_g mode in the M-fergusonite phase. Inset shows the calculated strain in the M-fergusonite phase as a function of the order parameter taking into account the calculated pressure dependence of the lattice parameters of the M-fergusonite phase plotted in Fig. 6.

Figure 7 shows that there is indeed a linear pressure dependence of the squared frequency of the soft $T(B_g)$ mode of the scheelite phase, located at 166 cm^{-1} at room pressure, up to the phase-transition pressure. This is in good agreement with the second-order nature of the scheelite-to-fergusonite phase transition. At the phase transition there is a change in sign in the pressure coefficient from negative to positive for the corresponding A_g mode in the fergusonite phase located at 153.5 cm^{-1} at 23.8 GPa. Both lines intersect at the critical pressure P_C of 23.3 GPa (a value close to the experimental transition pressure) and the values of κ_P and κ_F are −115 and 213 cm^{-2}/GPa, respectively. The absolute value of the slope ratio of these two modes in the high-pressure (ferroelastic) phase and low-pressure (paraelastic) phase is approximately 1.85; a value close to that expected for a classical displacive transition.[55] Furthermore, in ferroelastic transitions the scalar spontaneous strain, ε_S, near the critical pressure, P_C, should be proportional to the order parameter, η, with the order parameter being dependent on the pressure P as[54]

$$\eta = \sqrt{\frac{|P - P_C|}{P_C}}. \tag{8}$$

For YVO_4, we have calculated ε_S following Aizu's definition[56] using the calculated unit-cell parameters reported in Fig. 6(b) and assuming the theoretical transition pressure $P_C = 19$ GPa. The inset of Fig. 7 evidences that ε_S follows the linear relationship $\varepsilon_S = 0.0954\eta$; being the proportionality constant of the same order of magnitude that than obtained in tungstates and molybdates. The linear dependence of ε_S vs η in YVO_4 also suggests a second-order nature for the scheelite-to-fergusonite phase transition and reinforces the conclusion drawn from the analysis of the Raman soft mode in the scheelite phase. To conclude this discussion we would like to mention that the softening of the $T(B_g)$ mode in the scheelite phase implies a vanishing restoring force against

the corresponding deformation, which in turn should be related to the decrease in the scheelite C_{66} elastic constant beyond P_C.

V. CONCLUSIONS

We have performed RT Raman-scattering measurements and *ab initio* total-energy and lattice-dynamics calculations in YVO_4 up to 33 GPa. The pressure dependence of the experimental and calculated Raman-mode frequencies in the zircon and scheelite structures are reported and compared nicely with previous Raman-scattering measurements. The lack of Raman-active modes of the zircon phases is discussed and the previously unobserved Raman-active mode of the scheelite phase has been found. Indications of a second-order scheelite-to-fergusonite phase transition are experimentally observed above 20 GPa and supported by our theoretical calculations and by the application of Landau's theory of phase transitions. On decreasing pressure from 33 GPa the second-order displacive scheelite-to-M-fergusonite phase transition is found to be reversible unlike the first-order reconstructive zircon-to-scheelite phase transition that takes place around 7.5 GPa. Therefore, on fully releasing the pressure the sample remains metastable in the scheelite phase at ambient conditions.

Finally, we want to mention that indications of the subtle second-order phase transition in YVO_4 have been found in x-ray diffraction measurements under pressure up to 26 GPa.[19] Table I summarizes the calculated lattice parameters of the scheelite and fergusonite structures at theoretical 24.3 GPa. According to our calculated data, the scheelite-to-fergusonite transition should be easily detected in x-ray diffraction experiments covering a larger pressure range than Ref. 19. In particular, a clear indication must be the appearance of a weak peak corresponding to the (020) reflection of fergusonite at very low angles near 5°. New experiments are needed to further investigate the subtle second-order scheelite-to-fergusonite phase transition in YVO_4 and other vanadates. In particular, new high-pressure x-ray diffraction and photoluminescence measurements in rare-earth-doped YVO_4 at least up to 35 GPa would be needed.

ACKNOWLEDGMENTS

This work has been done under financial support from Spanish MEC under Projects No. MAT2006-02279, No. MAT2007-65990-C03-01/03, and No. CSD-2007-00045, and from "Vicerrectorado de Innovación y Desarrollo de la UPV" through Project No. UPV2008-0020. A.H.R. has been supported by CONACyT Mexico under projects No. J-59853-F and No. J-83247-F. Authors acknowledge B. Ferrand and S. Jandl for kindly providing YVO_4 bulk samples and Red Española de Supercomputación for providing computing time. Additionally, F.J.M. wants to express his gratitude to I. Loa for his help and to F. Rey, P. Concepción, and A. Sánchez for his help in allowing access and giving assistance in the Raman measurements performed at the Instituto de Tecnología Química in Valencia (Spain).

*Corresponding author. FAX: + 34 96 387 71 49; fjmanjon@fis.upv.es

[1] R. A. Fields, M. Birnbaum, and C. L. Fincher, Appl. Phys. Lett. **51**, 1885 (1987).
[2] A. K. Levine and F. C. Palilla, Appl. Phys. Lett. **5**, 118 (1964).
[3] T. Jensen, V. G. Ostroumov, J. P. Meyn, G. Huber, A. I. Zagumennyi, and I. A. Shcherbakov, Appl. Phys. B: Lasers Opt. **58**, 373 (1994).
[4] K. Riwotzki and M. Haase, J. Phys. Chem. B **102**, 10129 (1998).
[5] A. Huignard, T. Gacoin, and J. P. Boilot, Chem. Mater. **12**, 1090 (2000).
[6] M. Yu, J. Lin, Z. Wang, J. Fu, S. Wang, H. J. Zhang, and Y. C. Han, Chem. Mater. **14**, 2224 (2002).
[7] J. A. Baglio and G. Gashurov, Acta Crystallogr., Sect. B: Struct. Crystallogr. Cryst. Chem. **24**, 292 (1968).
[8] J. A. Baglio and O. J. Sovers, J. Solid State Chem. **3**, 458 (1971).
[9] S. A. Miller, H. H. Caspers, and H. E. Rast, Phys. Rev. **168**, 964 (1968).
[10] A. Chaves and S. P. S. Porto, Solid State Commun. **10**, 1075 (1972).
[11] E. J. Baran, M. E. Escobar, L. L. Fournier, and R. R. Filgueira, Z. Anorg. Allg. Chem. **472**, 193 (1981).
[12] B. M. Jin, S. Erdei, A. S. Bhalla, and F. W. Ainger, Mater. Res. Bull. **30**, 1293 (1995).
[13] Yu. K. Voron'ko, A. A. Sobol', V. E. Shukshin, A. I. Zagumennyĭ, Yu. D. Zavartsev, and S. A. Kutovoĭ, Phys. Solid State **51**, 1886 (2009).
[14] H. R. Xia, L. J. Hu, J. H. Zou, L. X. Li, X. L. Meng, L. Zhu, and W. T. Yu, Cryst. Res. Technol. **33**, 807 (1998).
[15] C. Z. Bi, J. Y. Ma, J. Yan, X. Fang, D. Z. Yao, B. R. Zhao, and X. G. Qiu, Eur. Phys. J. B **51**, 167 (2006).
[16] R. J. Elliot, R. T. Harley, W. Hayes, and S. R. P. Smith, Proc. R. Soc. London, Ser. A **328**, 217 (1972).
[17] D. L. Rousseau, R. P. Baumann, and S. P. S. Porto, J. Raman Spectrosc. **10**, 253 (1981).
[18] A. Jayaraman, G. A. Kourouklis, G. P. Espinosa, A. S. Cooper, and L. G. Van Uitert, J. Phys. Chem. Solids **48**, 755 (1987).
[19] X. Wang, I. Loa, K. Syassen, M. Hanfland, and B. Ferrand, Phys. Rev. B **70**, 064109 (2004).
[20] F. J. Manjón, D. Errandonea, J. López-Solano, P. Rodríguez-Hernández, S. Radescu, A. Mujica, A. Muñoz, N. Garro, J. Pellicer-Porres, A. Segura, Ch. Ferrer-Roca, R. S. Kumar, O. Tschauner, and G. Aquilanti, Phys. Status Solidi B **244**, 295 (2007).
[21] D. Errandonea and F. J. Manjón, Prog. Mater. Sci. **53**, 711 (2008).
[22] D. Errandonea, J. Pellicer-Porres, F. J. Manjón, A. Segura, Ch. Ferrer-Roca, R. S. Kumar, O. Tschauner, P. Rodriguez-Hernandez, J. Lopez-Solano, A. Mujica, A. Muñoz, and G. Aquilanti, Phys. Rev. B **72**, 174106 (2005).
[23] D. Errandonea, J. Pellicer-Porres, F. J. Manjón, A. Segura, Ch.

Ferrer-Roca, R. S. Kumar, O. Tschauner, P. Rodriguez-Hernandez, J. Lopez-Solano, A. Mujica, A. Muñoz, and G. Aquilanti, Phys. Rev. B **73**, 224103 (2006).
[24] F. J. Manjón, D. Errandonea, N. Garro, J. Pellicer-Porres, P. Rodríguez-Hernández, S. Radescu, J. López-Solano, A. Mujica, and A. Muñoz, Phys. Rev. B **74**, 144111 (2006).
[25] F. J. Manjón, D. Errandonea, N. Garro, J. Pellicer-Porres, J. López-Solano, P. Rodríguez-Hernández, S. Radescu, A. Mujica, and A. Muñoz, Phys. Rev. B **74**, 144112 (2006).
[26] R. Mittal, A. B. Garg, V. Vijayakumar, S. N. Achary, A. K. Tyagi, B. K. Godwal, E. Busetto, A. Lausi, and S. L. Chaplot, J. Phys.: Condens. Matter **20**, 075223 (2008).
[27] J. López-Solano, P. Rodríguez-Hernández, and A. Muñoz, High Press. Res. **29**, 582 (2009).
[28] D. Errandonea, R. Lacomba-Perales, J. Ruiz-Fuertes, A. Segura, S. N. Achary, and A. K. Tyagi, Phys. Rev. B **79**, 184104 (2009).
[29] A. B. Garg, R. Rao, T. Sakuntala, B. N. Wani, and V. Vijayakumar, J. Appl. Phys. **106**, 063513 (2009).
[30] F. J. Manjón, S. Jandl, G. Riou, B. Ferrand, and K. Syassen, Phys. Rev. B **69**, 165121 (2004).
[31] G. J. Piermarini, S. Block, and J. D. Barnett, J. Appl. Phys. **44**, 5377 (1973).
[32] D. Errandonea, Y. Meng, M. Somayazulu, and D. Hausermann, Physica B **355**, 116 (2005).
[33] K. Syassen, High Press. Res. **28**, 75 (2008).
[34] G. Kresse, M. Marshman, and J. Furthmüller (Computational Physics, Faculty of Physics, Universität Wien) have developed the computer code VASP. See http://cms.mpi.univie.ac.at/vasp
[35] J. P. Perdew, S. Burke, and M. Ernzerhof, Phys. Rev. Lett. **77**, 3865 (1996).
[36] P. E. Blöchl, Phys. Rev. B **50**, 17953 (1994); G. Kresse and D. Joubert, *ibid.* **59**, 1758 (1999).
[37] J. Zhang, J. Wang, H. Zhang, Ch. Wang, H. Cong, and L. Deng, J. Appl. Phys. **102**, 023516 (2007).
[38] K. Parlinski, computer code PHONON. See: http://wolf.ifj.edu.pl/phonon
[39] See supplementary material at http://link.aps.org/supplemental/10.1103/PhysRevB.81.075202 for calculation details regarding IR-active modes and its comparison to available experimental data.
[40] G. Herzberg, *Molecular Spectra and Molecular Structure II: Infra-Red and Raman Spectra* (D. Van Nostrand, New York, 1945).
[41] S. J. Duclos, A. Jayaraman, G. P. Espinosa, A. S. Cooper, and R. G. Maines, Sr., J. Phys. Chem. Solids **50**, 769 (1989).
[42] V. S. Stubican and R. Roy, Z. Kristallogr. **119**, 90 (1963); **34**, 1888 (1963).
[43] D. Errandonea, F. J. Manjón, M. Somayazulu, and D. Häusserman, J. Solid State Chem. **177**, 1087 (2004).
[44] K. Kusaba, T. Yagi, M. Kikuchi, and Y. Syono, J. Phys. Chem. Solids **47**, 675 (1986).
[45] M. Marqués, J. Contreras-García, M. Flórez, and J. M. Recio, J. Phys. Chem. Solids **69**, 2277 (2008).
[46] M. Flórez, J. Contreras-García, J. M. Recio, and M. Marqués, Phys. Rev. B **79**, 104101 (2009).
[47] A. Grzechnik, K. Syassen, I. Loa, M. Hanfland, and J. Y. Gesland, Phys. Rev. B **65**, 104102 (2002).
[48] A. Grzechnik, K. Friese, V. Dimitriev, H. P. Weber, J. Y. Gesland, and W. A. Crichton, J. Phys.: Condens. Matter **17**, 763 (2005).
[49] D. Errandonea, EPL **77**, 56001 (2007).
[50] D. Errandonea, R. S. Kumar, X. Ma, and C. Tu, J. Solid State Chem. **181**, 355 (2008).
[51] F. D. Hardcastle and I. Wachs, J. Phys. Chem. **95**, 5031 (1991).
[52] I. D. Brown and K. K. Wu, Acta Crystallogr., Sect. B: Struct. Crystallogr. Cryst. Chem. **32**, 1957 (1976).
[53] D. Errandonea and F. J. Manjón, Mater. Res. Bull. **44**, 807 (2009).
[54] L. D. Landau and E. M. Lifshitz, *Statistical Physics Part 1*, Course of Theoretical Physics Vol. 5, 3rd ed. (Pergamon, New York, 1994).
[55] M. A. Carpenter and E. K. H. Salje, Eur. J. Mineral. **10**, 693 (1998).
[56] K. Aizu, J. Phys. Soc. Jpn. **28**, 706 (1970).